EXPERIMENTAL STUDY OF PATH INDEPENDENCE OF THE J-INTEGRAL IN AN HSLA STEEL TENSILE PANEL[+]

D. T. Read[*], J. C. Moulder[*], and J. F. Cardenas-Garcia[*o]

The J-integral has been evaluated from full-field strain data from a double-edge-notched tensile panel of high strength low alloy (HSLA) steel. The specimen was 80 mm wide and 14 mm thick. The notch lengths were quite small, 1.5 mm. The strain measurement technique used was a newly developed video-optical method. The J-integral was evaluated using five series of paths: two rectangular with constant ratio of height to breadth; two rectangular with constant height and varying breadth; and one rectangular with constant breadth and varying height. The observed variation in J over different paths is 10 percent or less. The J-integral from the full-field strain measurement agreed with the J-integral measured from strain and CMOD gages.

INTRODUCTION

Fracture occurs when the driving force for fracture exceeds the material fracture resistance. Discussion continues on the identity of the most appropriate parameter to be used to characterize material fracture properties and fracture driving force. However it seems clear that the driving force for fracture, by any measure, is controlled by some combination of the stress-strain-displacement field surrounding the crack tip. Techniques for measurement of this field are therefore relevant to the measurement of the driving force for fracture, regardless of which fracture parameter eventually is judged the best.

* Fracture and Deformation Division, National Bureau of Standards, Boulder, Colorado 80303.

o Permanent address: Department of Mechannical Engineering, Colorado State University, Fort Collins, Colorado 80523.

One very widely used fracture parameter is the J-integral, developed by Rice (1) after Eshelby's pioneering work (2). The J-integral is

$$J = \int_{\Gamma} W dy - \vec{T} \cdot \partial\vec{u}/\partial x \, ds, \qquad (1)$$

where W is stress work density, $\int \sigma_{ij} d\varepsilon_{ij}$; σ_{ij} and ε_{ij} are the stress and strain tensors. $\vec{T}$ is the traction vector across the contour of integration, Γ, $\vec{u}$ is the displacement vector, ds is the increment of displacement along the contour of integration and x and y are Cartesian position coordinates, with the crack perpendicular to the y direction, propagating in the x direction.

The J-integral has been defined as a path independent line integral on a contour surrounding a crack tip; it has also appeared as the amplitude of the Hutchinson-Rice-Rosengren (HRR) stress-strain singularity (3,4). The original J-integral and a modified version have been used in tearing studies (5,6). The integral used in this paper is asserted to be the path-independent line integral J(1). No claim is intended here regarding the existence and/or amplitudes of HRR stress-strain fields in the present specimen, or about any unique correspondence between the J-integral measured here and the initiation or extent of tearing.

Furthermore, clarification of the term "fracture driving force" used above is necessary. J as defined by Equation (1) gives an actual crack driving force only under deformation theory plasticity, that is, linear or nonlinear elastic specimen behavior, as distinct from the familiar elastic and plastic deformation behavior of actual metals. In addition, Equation (1) assumes that only infinitesimal strains occur in the cracked body under consideration.

In actual metals, the J of Equation (1) is applied in unmodified form to contours away from the immediate neighborhood of the crack tip. This J is used as a parameter characteristic of the fracture process both before and immediately after the initiation of ductile tearing. The geometry dependence of the critical J value, J_{Ic}, for fracture initiation and the rate of change of J with progressive cracking have been studied extensively. A few examples of these studies may be found in References (7-9).

The frequent use of J as a fracture parameter has come about, in part, because it can be approximately calculated from the load-displacement record of deeply notched specimens of convenient geometries (10). Obtaining J from load-displacement information, instead of from the stress-strain-displacement terms indicated in Equation (1), is termed indirect measurement of J. Equation (1) has been used as written in many numerical analysis studies; a few examples are given in References (11-13).

Several investigators have discussed experimental determination of J by measuring of the stress, strain, and displacement terms indicated in Equation (1). Obtaining such information and using Equation (1) to get J is termed direct experimental measurement of J. Several reports of such procedures have appeared in the literature in recent years (14-17), although no comprehensive review is known to us.

Most direct measurements of J were based on data for a single path surrounding the crack tip. In some cases, symmetry assumptions were used, similar to those routinely used in numerical analysis. In these cases, only half of an actual path was instrumented, and symmetry allowed the total J to be obtained. Full-field strain data were used by Müller (18) to obtain J for multiple paths. This study used a difficult manual photoelastic technique to obtain data under load control.

The investigation reported here studied notches that were a small fraction (0.027) of the specimen width. Small cracks are important for structures because they may be overlooked accidentally, or, if discovered, they may be judged not to present a risk of fracture. However, small cracks present experimental difficulties because the crack-related strains occur over a smaller area than for large cracks. A recent study reported that the notch size significantly affected the form of the dependence of J on applied strain (19).

Full-field strain data were used for direct measurement of J via Equation (1), on a double-edge-notched tensile specimen of a high-strength, low-alloy (HSLA) steel. A new technique for obtaining full-field, in-plane strain data was applied. Measurements from a variety of paths were used to study the path independence of J and were compared with the results from direct measurements of J using a previously reported technique involving strain gages along a selected contour (15).

MATERIAL

The specimen material used in this investigation was reported by the manufacturer to be ASTM A710 Grade A Class 3 alloy steel. It was received in the form of 19 mm (0.75 in) thick plate. The chemical analysis, as supplied by a commercial source, is listed in Table 1. This analysis indicates less than 0.01 weight percent of Nb, which violates the specification for A710 Grade A Class 3 steel. Some unusual behavior of this alloy under heat treatment, which may be related to its chemistry, has been noted (20). The tensile properties of the specimen material, obtained using replicate round bar tensile specimens 6.4 mm (0.25 in) in diameter, are listed in Table 2. The engineering stress-strain curve, given in Figure 1, contains a slight yield point, some Lüders extension, and strain hardening. The tensile properties of the specimen material

at room temperature were essentially the same in the transverse and longitudinal directions, except for the elongation, as can be seen from Table 2. The Lüders strain after the yield point was present in both longitudinal and transverse orientations. After its maximum, the load decreased more rapidly with extension in the longitudinal specimens than in the transverse ones; this led to the lower elongation values for the longitudinal specimens.

TABLE 1. Chemistry analysis in weight percent, of the ASTM A-710 specimen material used in the present study.

Carbon	Manganese	Nickel	Chromium	Silicon	Copper	Sulfur
0.042	1.54	1.85	0.65	0.34	1.2	0.010

Phosphorus	Niobium	Aluminum
< 0.005	< 0.010	< 0.020

TABLE 2. Tensile properties of the ASTM A-710 Grade A steel alloy used in the present study, measured on round tensile bars.

Longitudinal		
Yield Strength, 0.2 percent offset	637 MPa	92.4 ksi
Ultimate tensile strength	732 MPa	106.2 ksi
Elongation	12.0 percent	
Reduction of Area	75.5 percent	
Tranverse		
Yield Strength 0.2 percent offset	634 MPa	92.3 ksi
Ultimate tensile strength	727 MPa	105.3 ksi
Elongation	17 percent	
Reduction	71 percent	

The fracture toughness of this specimen material at room temperature was investigated using three-point-bend specimens in the TL and LT orientations. Items of noncompliance with ASTM standard method E-813, which was used for the toughness tests, were the differences between compliance-measured and physical crack extension values, Δa_c and Δa_p, and the specimen dimensions. The higher values of J used to obtain the material tearing modulus failed to meet the specimen size requirement.

The results of the J-integral tests indicate that the specimen material is quite tough at room temperature, and that non-side-grooved specimens without side grooves and with the LT orientation (crack grows across the rolling direction) are the toughest (J_{Ic} = 374 N/mm, T_{mat} = 177), while side-grooved specimens in the TL orientation (crack grows along the rolling direction) are the least tough (J_{Ic} = 128 N/mm, T_{mat} = 48). No pop-ins or other signs of rapid crack advance were observed in these room temperature tests. In the TL orientation, the side-grooved and non-side-grooved specimens had similar J_{Ic} values. However in the LT orientation, the one side-grooved specimen had lower J_{Ic} and T_{mat} values than the two non-side-grooved specimens.

SPECIMEN AND CONVENTIONAL DIRECT J-INTEGRAL MEASUREMENT METHOD

A tensile panel specimen for direct J measurement was machined with a gage section measuring 82 mm (3.22 in) wide by 14 mm (0.55 in) thick by 250 mm (10 in) long. The total specimen length was 850 mm (33 in), oriented along the rolling direction. The grip sections at each end of the specimen were 108 mm (4.25 in) wide to confine plastic strain to the gage section. Mechanical wedge grips clamped the specimen grip sections.

Instrumentation as described previously (15) for direct measurement of the J-integral by strain gages along a selected contour was used, including a load cell built into the testing machine, a crack mouth opening displacement (CMOD) gage (ring-gage), 36 electrical resistance strain gages, and up to three linear variable differential transformer (LVDT) gages for displacement measurement. An array of five small strain gages was located near the crack mouth to give the strain profile there, as shown in Figure 2. Some gages were located away from the crack, for measurement of remote strain.

The instrumentation for recording strain gage strains, load, crack mouth opening displacement, and LVDT displacement has been described elsewhere (15).

In the post-test data analysis, all the measured values of strain and displacement were zero corrected by fitting the linear part of the record for each quantity to a linear dependence on the stress, then forcing zero strain or displacement at zero stress by

offsetting the measured strain or displacement. The J-integral was calculated using the trapezoidal rule for displacement and stress-work integrals along both sides of the contour. Because the contours were chosen along specimen edges so that the stresses at the contour were uniaxial, an elastic-perfectly-plastic approximation of the simple round-bar stress/strain curve was used for calculating stress-work.

Integration of strain gage strains to obtain the displacements needed for calculation of the traction-bending term of the J-integral gave some error cancellation, which would not have been obtained had the LVDT displacements been used. The LVDT displacements were used to check the integrated strain values and for gage length strain measurement after strain gage failure.

Good correlations were obtained experimentally between the J-integral and a reference quantity, J_{ref}, given by

$$J_{ref} = 1.0 \times \sigma_f \times \text{CMOD} \quad . \tag{2}$$

Here σ_f is the material flow strength, the mean of the yield and ultimate strengths, and CMOD is crack mouth opening displacment. This correlation is expected because of low geometrical constraint of the simple tension geometry used here. After strain gage failure, this correlation was used to obtain J-integral values.

The analytical approach and experimental techniques used to obtain the J-integral were discussed at length in a previous report (15). It was concluded that uncertainty in the measured J-integral values themselves was about ±10 percent and that material variability could raise this uncertainty in specimen-to-specimen comparisons.

FULL-FIELD STRAIN-MEASUREMENT TECHNIQUE

A new method for measuring entire two-dimensional strain fields has been developed. A complete description will be published elsewhere (21). The technique is based on the automated analysis of optical diffraction patterns formed by a laser beam passed through photographic negatives of deformed specimen grids. A block diagram of the system is shown as Figure 3.

In common with moiré analysis, the method requires that a grid be applied to the surface of the object under study; however, the method of analysis is completely different from conventional moiré methods. Photographs are taken of the specimen grid in the undeformed state and in the deformed state. The photographic negative of a deformed specimen grid is analyzed by passing a laser beam through the negative and forming the far field (Fraunhofer) diffraction pattern with a positive lens. The diffraction pattern is imaged with a solid state video camera and the image is digitized

and stored with a video digitizer. A desktop computer interfaced to the video digitizer determines the locations of the centroids of the first-order diffraction peaks. From these peak locations, the strains are calculated.

The centroid location X^k is calculated from

$$X^k = \frac{\sum_{i=1}^{m} \sum_{j=1}^{n} I_{ij} \, X^k_{ij}}{\sum_{i=1}^{m} \sum_{i=1}^{n} I_{ij}} , \qquad (3)$$

where each (i,j) indicates one element (pixel) of the digitized image, I_{ij} is the pixel intensity, ranging from 0 to 255, X^1 = x position and X^2 = y position. The summations are performed in a 19 x 19 pixel window surrounding each spot, with the background subtracted from each I_{ij} so that only pixels that form the spot have nonzero intensity.

The centroids of the four first-order diffraction peaks are compared for deformed and undeformed grids as shown in Fig. 4. In-plane strains are then calculated using

$$\varepsilon_{xx} = \frac{X^1 - X^{1'}}{X^{1'}} \qquad (4a)$$

$$\varepsilon_{yy} = \frac{X^2 - X^{2'}}{X^{2'}} \qquad (4b)$$

$$\gamma_{xy} = \frac{\alpha + \beta}{2} \qquad (4c)$$

$$\theta = \frac{\alpha - \beta}{2} \qquad (4d)$$

where (see Figure 4) the prime indicates centroid location for the deformed grid. This analysis yields all four in-plane components of the deformation tensor: longitudinal strain ε_{yy}, transverse strain ε_{xx}, shear strain γ_{xy}, and rigid body rotation θ. Evaluation of the entire deformation field is accomplished by analyzing the photograph point by point.

In the present study, optical components appropriate for a proof-of-principle study were used. An 80-line-per-centimeter grid was bonded to the specimen. The rectangular grid was placed with

one edge just below the crack plane, centered between the specimen edges. The active grid area was 80 mm by 100 mm.

Photographs of the deformed grid were taken at several strain levels, using a 35 mm camera with a good quality commercial macro lens and high resolution black and white film. No special precautions were taken during development of the film. Two photographs were analyzed in detail. The 80 mm by 100 mm field was analyzed on a grid of 15x16 points.

The method described above was implemented with the optical system shown in Fig. 3. The laser was a 3 mW HeNe laser with an output beam diameter at the 1/e points of 0.8 mm. The Fourier transform lens L-1 was a 75 mm diameter two element positive lens with a focal length of 15.8 cm. The diffraction pattern of the grid was formed on a ground glass screen located at the focal point of L-1. This pattern was in turn imaged with a solid state CCD video camera with a macro lens. The use of a camera lens and ground glass permitted adjustments to the position of the camera to optimize the image size of the diffraction pattern.

The video signal from the CCD camera was digitized with a video frame-store. The video digitizer could store a single frame in two fields of 256 x 256 pixels each with 8 bits of resolution (256 gray levels). The data were transferred to a desk top computer via a 16-bit parallel bus with direct memory access.

Input of data from the video digitizer and all computations of spot centroids and positions were accomplished with a desktop computer programmed in BASIC. Total time required to perform these operations for a single point in the image was 40 seconds. The photograph of the grid was positioned manually in the laser beam with a 3-axis micropositioner. To analyze an entire field, the photograph was stepped across the laser beam in a raster of 1 mm increments covering the entire field. This operation could easily be automated by the addition of a two-axis, computer-controlled positioner.

The main advantage of the present technique is that all four components of the in-plane deformation tensor are obtained rapidly for strain levels up to about 5 percent without laborious and time-consuming manual reduction of data.

Limitations of this new technique, as currently implemented, are principally its low precision, compared to electrical resistance strain gages, and low spatial resolution. The current precision is about 0.2 percent strain. This represents an ideal precision at a location where the strain field is nearly uniform. The relatively low precision of the strain measurement is thought to be the result of using a ground glass screen to image the diffraction pattern. Using a relay lens at the focal plane of L-1

(Figure 3) to image the diffraction pattern directly on the CCD-sensor would eliminate the need for the ground glass and so would probably permit a much more accurate determination of diffraction peak centroids and improved precision in the strains measured.

The low spatial resolution results from the use of 35 mm film to record the grid images coupled with use of a 1-mm-diameter laser beam to interrogate the images. The grid line density on the negative was about 400 lines/cm, which is approximately the maximum possible resolution of the camera-lens system used. This combination resulted in about a 5 mm spatial resolution for strains in the present study. This resolution was sufficient everywhere except in the neighborhood of the crack mouth. For this single point, strain information was supplemented by information from strain gages. Errors larger than 0.2 percent in strains measured near the crack mouth are believed to have occurred. See the Discussion, below.

CALCULATION OF J-INTEGRAL

As shown by Müller (18), the evaluation of the integral of (1) requires strains, stresses, and displacement gradients as input data. The raw measured data from the video-optical system gives the axial strains, ε_{xx} and ε_{yy}, directly under the assumption of small strains. Shear strains are trivially obtained from the angular strain γ_{xy}. Certain needed displacement gradients are identical to ε_{xx} and ε_{yy}. The others, for example, $\partial u_y/\partial x$, were obtained as linear combinations of the shear strain and the rotation. To eliminate systematic errors of alignment, the average rigid body rotation over the full field was forced to zero.

Stresses were calculated from measured strains by assuming that the mechanical behavior of the isotropic, elastic, strain hardening plate material subjected to small, time independent, isothermal deformation (with no unloading) can be approximated by deformation plasticity theory. Assuming that the small plastic deformation is incompressible and isotropic and that the loading is proportional, we can then, by the usual elastic-plastic strain decomposition, relate the elastic and plastic strains to the final states of stress by a generalized Hooke's Law, the Mises yield criterion, and Prager's isotropic strain hardening rule, which is the simple power rule, (22-24). For the uniaxial case these final stress-strain relations reduce to the Ramberg-Osgood formulation. The usual deformation-theory-plasticity expression for the strain energy density was used.

The J-integral calculation is then made for plane stress conditions, from the experimentally determined strains and displacement gradients and the calculated stresses and stress work density.

RESULTS

The J-integral was evaluated for each of the two edge notches using five series of rectangular paths: two of fixed height (varying width), two of fixed width (varying height), and self similar, (width and height vary together). Figure 5 shows the results for remote axial strain plotted against remote stress. Remote here means the instrumentation furthest from the crack plane. Remote stress is applied load divided by uncracked cross-sectional area. The two data points at which full-field data were obtained are indicated in Fig. 5 by arrows. The average values of axial strains are about 0.018 and 0.028, both well above the yield strain of 0.0031.

Figure 6 shows the distribution of axial strain over the measured field. In this image, the strain is proportional to brightness, ranging from 0 (black) to 4 percent (white). Each small square in the image corresponds to an area of 25 square mm on the panel.

Figure 7 shows a photoelastic image of the same strain field, taken in white light and reproduced in monochrome.

Calculated J-integrals are shown in Table 3 for a series of five paths.

Table 3. J-integral values for five series of paths around the left crack at a remote strain of 0.037.

Path Height mm	Path Width, mm	Average J, N/mm	Average deviation from average J, percent (%)
Width x 2	5.4 to 32	222	6.1
10.8	10.8 to 32	212	8.0
27	10.8 to 32	250	2.5
10.8 to 75	10.8	228	3.4
10.8 to 75	32	214	9.1
	AVERAGE	225	5.8

DISCUSSION

The variability of measured J-values evident in Table 3, both on each series of paths and among the series, is not negligible. Examination of the results indicated that this variability appeared to be simple scatter. No consistent trends in J with path size were detected. An important possible cause for path dependence could be nonproportional loading, which would invalidate the theoretical proof of path-independence of J (25). As noted above, the stress-strain behavior of steel in general is clearly inconsistent with deformation theory plasticity. However, if an actual material is loaded proportionally without unloading, its behavior is indistinguishable from deformation theory plasticity. Therefore, path dependence of J could indicate nonproportional loading. In fact, J is known to be path dependent close to the tips of growing cracks, because of local nonproportional loading. However, the cracks used in the present study were blunt, because they were simply cut with a saw, and no systematic changes in J near the crack tips were observed. Therefore, the variability of J observed in the present study is not attributed to nonproportional loading.

Limitations on the spatial resolution and precision of the full-field strains measured here were mentioned above. Errors in these strains would produce errors in the calculated J values. A check showed that a +1 percent change in ε_{yy} at the first measurement point above the crack mouth produced a change of -100 N/mm here. Combinations of strain errors up to 0.1 percent strain at each point along a contour could easily produce the path dependence observed.

As a further check, the crack mouth opening displacement (CMOD) implied by the measured displacement gradients was calculated by integrating around several J contours. The variability of the CMOD was larger than the variability of J. The variability of the CMOD can only result from accumulation of errors around the integrations paths. The source of these errors is the errors of measurement of displacement gradients. The same source produces the variability of J.

Table 4 compares the full-field J, J_{ff}, results for the two cracks in the DEN specimen at two strain levels with J values obtained from strain gage strains, J_{sg}, and with the quantity $J_{ref} = \sigma_f * CMOD$, where CMOD was measured by a clip gage and σ_f is the mean of the yield and ultimate strengths, and with a theoretical estimate of J, J_{est} (25,26).

The estimated J value for the lower remote strain value is very low because the remote strain is low. The local strain around the crack tip is around 0.02, but the Lüders strain has not propagated out to the remote strain gage. These complexities are discussed in (27).

This table shows fortuitously good agreement among the full field J, the strain gage J, the quantity J_{ref}, and the estimated J for the left crack at the higher strain level. Poorer agreement exists among these quantities at the lower strain level and between the values for the left and right cracks at both strain levels.

Table 4. Summary of full-field, strain gage, and estimated J values and related quantities.

Crack	J_{ff} (N/mm)	J_{sg} (N/mm)	CMOD (N/mm)	σ_f*CMOD (N/mm)	Remote strain	J_{est} (N/mm)
left	173	139	0.181	124	0.0032	10
right	205	-	-	-	0.0032	10
left	225	229	0.329	225	0.037	228
right	316	-	-	-	0.037	228

Because all J-integral paths must begin and end on the crack flanks, possibly at the crack mouth, the strain values near the crack mouth are critical to obtaining accurate full-field J values. Table 4 shows that the J values at the higher strain level for the left and the right cracks differed by 40 percent. Similar differences occurred at the lower strain value. The reason for these difference is unknown. The two possibilities are experimental error or actual differences between the J integral for the two cracks. The available data are insufficient to indicate which of these two possibilities is correct.

SUMMARY AND CONCLUSION

In this paper full field strain measurements were used to obtain the J integral by path integration for very short cracks (1.5 mm) at very high strain levels (0.04 ~ 14 x yield). The spatial resolution was about 5 mm and the strain resolution was about 0.1 percent (≈ 3 x yield stress). Strain data at one point 5 mm above the crack mouth were obtained from strain gage results because the full-field strain results were obviously erroneous at that point. For this strain level, variability of up to 10 percent was observed for five series of paths. The differences among the series averages ranged up to 11 percent for the best data set and were higher for the others. This variability is ascribed entirely to experimental errors. No path dependence of J is observed.

The J value obtained from the best data set turned out to be quite accurate, with an error in the neighborhood of 2 percent. However, differences of up to 40 percent were observed between the left and right cracks. We were unable to determine whether these differences resulted from experimental error or from actual differences in J between the two cracks.

This study shows that J-integral measurement using a video-optical full field strain measurement is a useful research tool. The path independence of Rice's J integral was verified to within 10 per cent under the unusual conditions of very large plastic strains and very small crack sizes. However, this study also shows that strain data with errors small compared to the yield strain and with spatial resolution over distances small compared to the crack length are needed, at least near the crack mouth, if accurate J-integral values are to be obtained consistently.

ACKNOWLEDGMENTS

Financial support of the Fracture Control Technology Program of the U. S. Naval Sea Systems Command, under Project Monitor J. P. Gudas, is gratefully acknowledged. Technical assistance by J. D. McColskey in setting up the test and B. Gunther in taking full-field strain data is appreciated.

REFERENCES

(1) Rice, J. R., "A Path Independent Integral and the Approximate Analysis of Strain Concentration by Notches and Cracks," J. Appl. Mech., Vol. 35, 1968, pp. 379-386.

(2) Eshelby, J. D., "The Continuum Theory of Lattice Defects," in Solid State Physics, Vol. III, pp. 79-144, Academic Press, New York, 1969.

(3) Hutchinson, J. W., "Singular Behavior at the End of a Tensile Crack in a Hardening Material," J. Mech. Phys. Solids, Vol. 16, 1968, pp. 13-31.

(4) Rice, J. R., and Rosengren, G. F., "Plane Strain Deformation Near a Crack Tip in a Power Law Hardening Materials," M. Mech. Phys. Solids, Vol. 16, 1968, pp. 1-12.

(5) Paris, P. C., Hada, H., Zahoor, A., and Ernst, H., "The Theory of Instatibility of the Tearing Mode of Elastic-Plastic Crack Growth," in Elastic-Plastic Fracture. ASTM STP 668, J. D. Landes, J. A. Begley, and G. A. Clarke, Eds., American Society for Testing and Materials, 1979, pp. 5-36.

(6) Ernst, H. A., "Material Resistance and Instability Beyond J-Controlled Crack Growth," in Elastic-Plastic Fracture:

Second Symposium, Volume I - Inelastic Crack Analysis, ASTM STP 803, C. F. Shih and J. P. Gudas, eds., American Society for Testing and Materials, 1983, pp. I-191-I-213.

(7) Landes, J. D., and McCabe, D. E., "Effect of Specimen Size and Geometry on Ductile Fracture Characterization," Proceedings of the Third International conference on Mechanical Behavior of Materials, Pergamon Press, Oxford, 1979, pp. 539-547.

(8) Vassilaros, M. G., Joyce, J. A., and Gudas, J. P. "Effects of Specimen Geometry on the J-R Curve for ASTM A533B Steel," Fracture Mechanics: Twelfth conference, ASTM STP 700, American Society for Testing and Materials, Philadelphia, 1980, 251-270.

(9) Kaiser, H.-J., and Hagedorn, K. E., "The Influence of Specimen Geometry on Stable Crack Growth for a High-Strength Steel." Advances in Fracture Research, Volume 2, Pergamon Press, Oxford, 1982, pp. 833-841.

(10) Rice, J. R., Paris, P. C., and Merkle, J. G., "Some Further Results of J-Integral Analysis and Estimates, " in Progress in Flaw Growth and Fracture Toughness Testing, ASTM STP 536, American Society for Testing and Materials, Philadelphia, 1973, pp. 231-245.

(11) McMeeking, R. M., and Parks, D. M., "On Criteria for J-Dominance of Crack-Tip Fields in Large-Scale Yielding," Elastic-Plastic Fracture ASTM STP 668, J. D. Landes, J. A. Begley, and G. A. Clarke, eds., American Society for Testing and Materials, Philadelphia, 1979, pp. 175-194.

(12) Hilton, P. D., and Gifford, L. N., "Elastic-Plastic Finite-Element Analysis for Two-Dimensional Crack Problems," Elastic-Plastic Fracture: Second Symposium, Volume I-Inelastic Crack Analysis, ASTM STP 803, C. F. Shih and J. P. Gudas, eds., American Society for Testing and Materials, Philadelphia, 1983, pp. I-256-I-273.

(13) Dodds, R. H., and Read, D. T., "Experimental Analytical Estimates of the J-Integral for Tensile Panels Containing Short Center Cracks," International Journal of Fracture, Vol. 28, 1985, pp. 39-54.

(14) Tirosh, J., and Berg, C. A., "Experimental Stress Intensity Factor Measurements in Orthotropic Composites," Composite Materials: Testing and Design (Third Conference), ASTM STP 546, American Society for Testing and Materials, Philadelphia, 1974, pp. 663-673.

(15) Read, D. T., "Experimental Method for Direct Evaluation of the J-Contour Integral," Fracture Mechanics: Forteenth Symposium-

Volume II: Testing and Applications, ASTM STP 791, J. C. Lewis and G. Sines, eds., American Society for Testing and Materials, Philadelphia, 1983, pp. II-199-II-213.

(16) Kawahara, W. A., and Brandon, L., "J-Integral Evaluation by Resistance Strain Gauges," Engineering Fracture Mechanics, Vol. 18, 1983, pp. 427-434.

(17) Frediani, A., "Experimental Measurement of the J-Integral," Engineering Fracture Mechanics, Vol. 19, 1984, pp. 1105-1137.

(18) Müller, T. "Experimentelle Untersuchung Der Wegungabhängigkeit des J-Integrals Bei Grossen Plastischen Zonen," Dissertation, Technische Hochshule Darmstadt, 1980.

(19) Read, D. T., "Applied J-Integral Values in Tensile Panels," in Ductile Fracture Test Methods, Proceedings of a CSNI Workshop, Paris, December 1982, Organization for Economic Co-Operation and Development, Paris, pp. 273-291.

(20) Personal communication, R. J. Fields, National Bureau of Standards, Gaithersburg, Maryland.

(21) Moulder, J. C., to be published.

(22) Prager, W., "Strain Hardening Under Combined Stres," Journal of Applied Physics, Vol. 16, 1945, pp. 837-840.

(23) Budiansky, B., "A reassessment of Deformation Theories of Plasticity," Journal of Applied Mechanics, Vol. 26, 1959, pp. 259-264.

(24) Lee, J. D., and Liebowitz, H., "The Nonlinear and Biaxial Effects on Energy Release Rate, J-Integral and Stress Intensity Factor," Engineering in Fracture Mechanics, Vol. 9, 1977, pp. 765-779.

(25) Rice, J. R., "Discussion: The Path Dependence of the J-Contour Integral, by G. G. Chell and P. T. Heald," International Journal of Fracture, Vol. 11, 1975, pp. 352-353.

(26) Begley, J. A., Landes, J. D., and Wilson, W. K., "An Estimation Model for the Application of the J-Integral," Fracture Analysis, ASTM STP 560, American Society for Testing and Materials, Philadelphia, 1974, pp. 155-169.

(27) Wilson, W. K., "J-Integral Estimate for Small Edge and Interior Cracks," Engineering Fracture Mechanics, Vol. 20, 1984, pp. 655-665.

(28) Read, D. T., "Applied J-Integral Values for Small Cracks in Steel Panels," presented at 18th National Symposium on Fracture Mechanics, Boulder, Colorado, June, 1985.

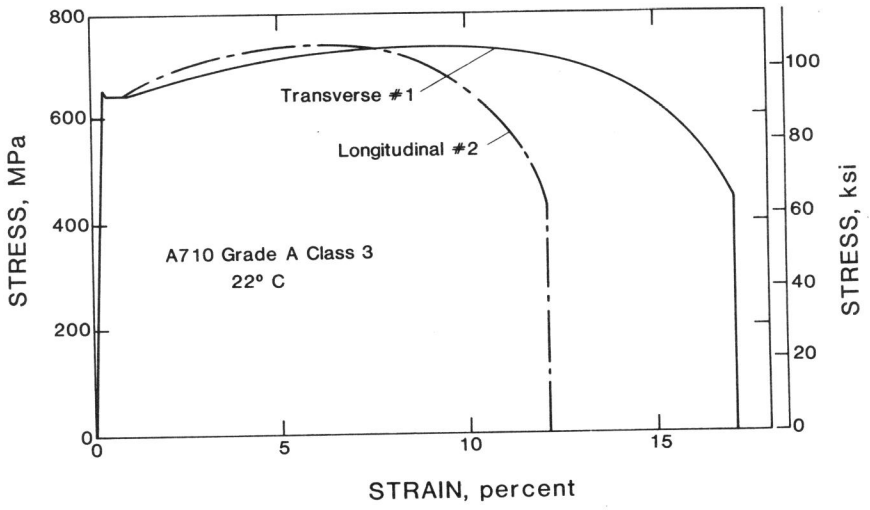

Figure 1. Engineering stress-strain curves of longitudinal- and transverse-oriented tensile specimens of the ASTM A710 Grade A Class 3 material used in this study.

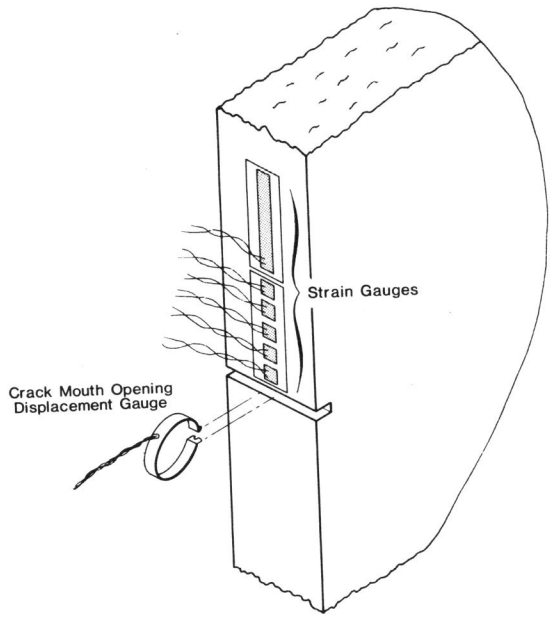

Figure 2. Near-crack-mouth instrumentation for direct measurement of J-integral.

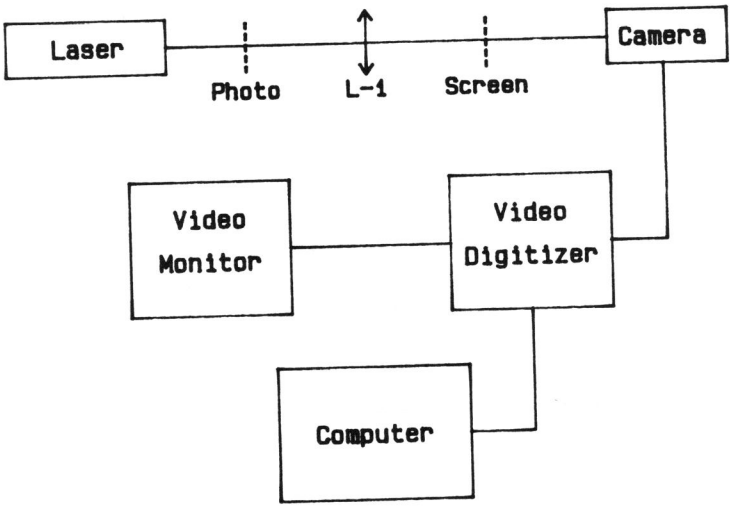

Figure 3. Block diagram of full-field strain measurement apparatus.

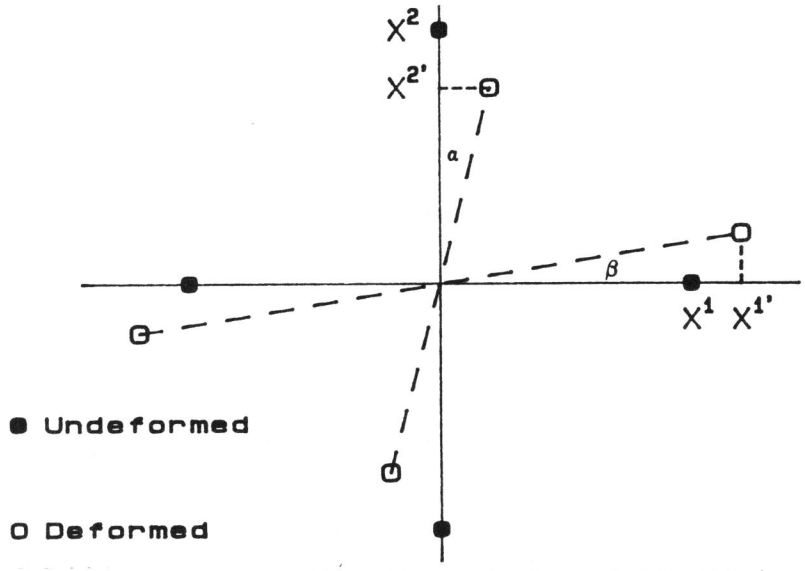

Figure 4. First-order diffraction peaks for undeformed and deformed grids.

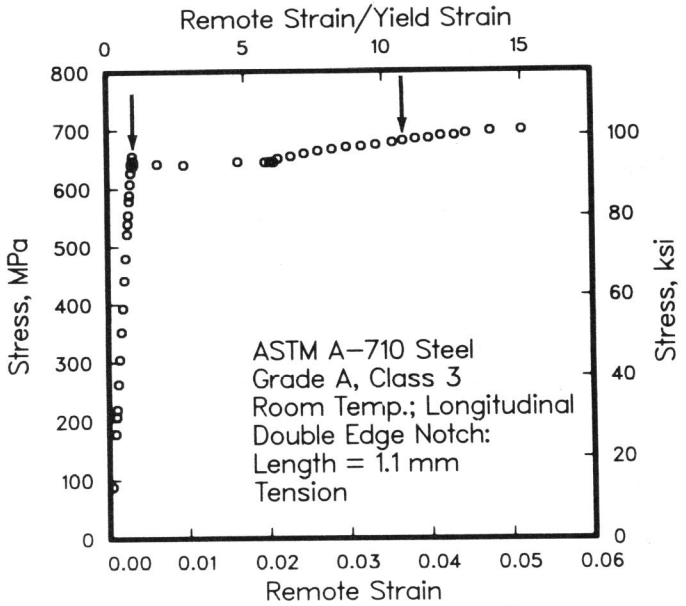

Figure 5. Plot of remote axial strain against stress, showing strains at which full field strain data were obtained.

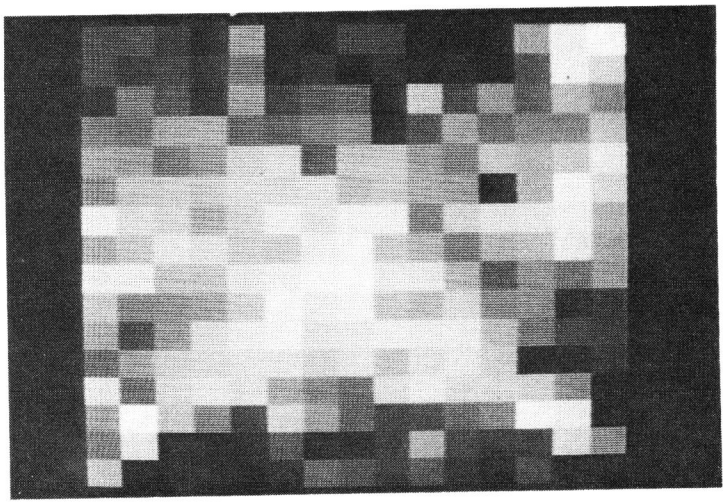

Figure 6. Distribution of axial strain at a remote strain of 0.037. The strain ranges from zero (black) to 4 percent (white).

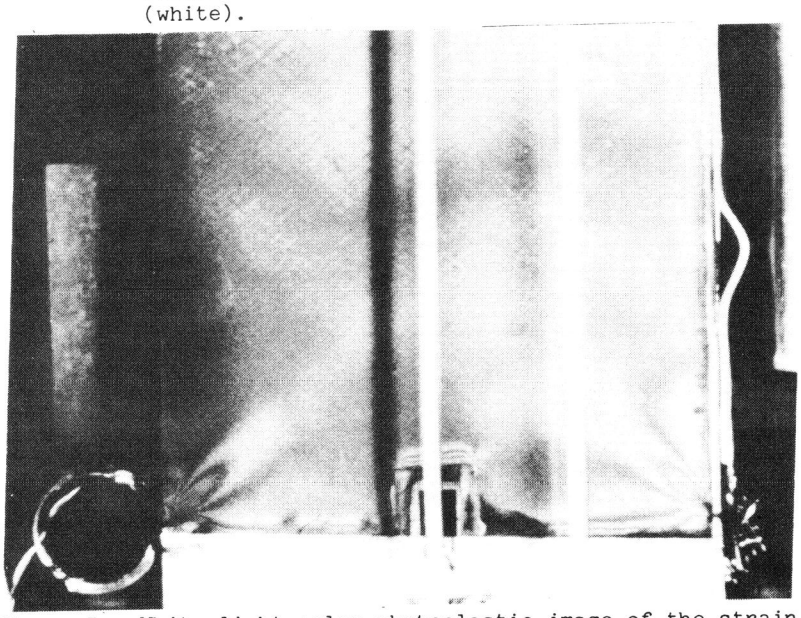

Figure 7. White-light color photoelastic image of the strain field a remote strain of 0.037.